On the Wave Propagation in Hydroelastic Phononic Crystals

Vinícius Mauro de Souza Santos[1,2][0000−0001−7292−9394], Romain Viala[2][0000−0001−5352−210X], Thiago de Paula Sales[1][0000−0002−5988−167X], and Morvan Ouisse[2][0000−0001−5464−5283]

[1] Mechanical Engineering Division, Aeronautics Institute of Technology, Praça Marechal Eduardo Gomes, 50 - Vila das Acácias, 12228-900, São José dos Campos, SP, Brazil

[2] Université Marie et Louis Pasteur, SUPMICROTECH, CNRS, Institut FEMTO-ST, F-25000, Besançon, France

vinicius.santos@ga.ita.br, romain.viala@femto-st.fr, tpsales@ita.br, morvan.ouisse@femto-st.fr

Abstract. Phononic crystals (PCs) and elastic metamaterials (EMs) have been viewed as innovative solutions for wave manipulation in various applications. By exploiting periodicity, engineering structures can be designed to enable various interesting functionalities such as bandgap formation, energy localization, "diode" mechanisms, and more which are not readily found in conventional materials. Accordingly, this paper develops a modeling technique for hydroelastic PCs, combining reduced-order unit cell models with the Wave-based Finite Element Method (WFEM), and investigates the influence of fluid filling levels on their dynamic behavior. The baseline unit cell is three-dimensional and features an internal void that allows the confinement of fluid (water) within its structure. Results from numerical simulations illustrate the good accuracy of reduced-order models and the WFEM in predicting the dynamic behavior of hydroelastic PCs. Besides, dispersion analyses and forced responses showed that the propagation of waves is significantly affected by varying the fluid filling level, shifting stopbands and enhancing bandgap formation. Therefore, this work opens new avenues for the design of advanced metastructures with strong potential for wave manipulation, including tunable bandgaps and waveguides, adaptive vibration control, reconfigurability, and other functions.

Keywords: Hydroelastic phononic crystals · Model order reduction · Wave-based finite element method.

1 Introduction

Periodic structures have attracted increasing interest over the years due to their ability to manipulate wave propagation for various applications. Typically designed using repetitive units, known as unit cells, periodic structures can exhibit spatial periodicity in one, two, or three dimensions, giving rise to the so-called

phononic crystals (PCs) or elastic metamaterials (EMs). These engineered systems are commonly used to passively control vibrations, offering novel and advanced strategies for vibration mitigation and control.

The literature abounds with studies on periodic structures for various purposes. Khelif et al. [1], for example, designed a two-dimensional (2D) PC to guide ultrasonic waves by exploiting specific patterns of defects. Li et al. [2] investigated the dispersion relations of fluid-filled PCs with both weak and strong fluid-structure coupling. Spadoni et al. [3], in turn, focused on the dynamic behavior of closed-cell crystalline foams and demonstrated that they exhibit superanisotropic properties, behaving either as a fluid or a solid. Dorodnitsyn and Spadoni [4] studied wave propagation within micrometer-scale poroelastic PCs. The same authors also investigated elastic wave propagation in 2D porous and cellular (non-porous) micrometer-scale square PCs, with and without entrained fluid in the former [5].

Dorodnitsyn and Damme [6] investigated an acoustic metamaterial with a negative refraction index incorporating entrained fluid. Jensen and Kook [7] studied the existence of coupled elasto-acoustic bandgaps in corrugated plate structures and acoustic channels. The dynamic behavior of hollow pillars selectively filled with water and periodically arranged on a square foundation was considered by Wang et al. [8], who also investigated acoustoelastic resonators consisting of a solid matrix with fluid-filled cavities for the design of reconfigurable phononic circuits [9]. Later, Zhang et al. [10] developed a tunable acoustoelastic metamaterial consisting of local resonators hosted in plate-like unit cells.

Afterwards, Elmadih et al. [11] investigated simultaneous acoustic and elastic bandgaps in PCs composed of solid and fluid (air) media. Yu et al. [12] designed a PC pipe by exploiting Bragg scattering and local resonance phenomena in pursuit of vibration reduction. Dai et al. [13] also investigated the dynamic behavior of periodic fluid-conveying pipes for similar purposes. Helmholtz resonators, periodically arranged in a fluid-filled pipe, were studied by Yu et al. [14]. Hu et al. [15] similarly investigated vibration control in a locally resonant fluid-conveying pipe system, but by exploiting both Bragg and resonant-type bandgaps.

Although numerous works exist on the dynamic behavior of a variety of PCs and EMs, not much is known about hydroelastic PCs — i.e., periodic structures that combine solid and liquid media. Hydroelastic metamaterials can offer several advantages over conventional PCs, as well as more sophisticated metamaterials that incorporate piezoelectric patches or other technologies, for instance. To name a few: (1) hydroelastic PCs can allow for continuous tuning of their mass, which might be achieved by altering the fluid level within the lattice; (2) hydroelastic PCs are highly versatile due to the shapeless nature of fluids, which allows them to conform to virtually any cavity or geometry, even highly complex ones, thereby enhancing their applicability across a wide range of problems; (3) a broad range of parameters governs the coupling intensity between elastic and pressure waves in hydroelastic PCs, such as the fluid level and type, the geometry and material of the host unit cell, and even magnetic forces in magnetorheological fluids [16], thus enabling a highly flexible design of this interesting class of

metamaterials for wave manipulation. All these features make hydroelastic PCs promising alternatives for vibration control, especially in applications involving water availability, such as those in oceans, among other environments.

In this respect, this work investigates the dynamic behavior of hydroelastic PCs with one-dimensional periodicity, taking into account the occurrence of fluid sloshing in partially filled unit cells. The baseline unit cell is three-dimensional and features an internal void that allows the confinement of fluid (water) within its structure [17], as shown in Fig. 1 for three different fluid filling levels. Numerical simulations are carried out using the Wave-based Finite Element Method (WFEM), combined with a novel model order reduction (MOR) scheme that accelerates simulations and mitigates the occurrence of numerical issues commonly encountered in the WFEM. Due to sloshing at the fluid free surface in partially filled unit cells, pressure variations are induced in the surrounding medium, and therefore, one accounts for such an effect as increased inertia [18].

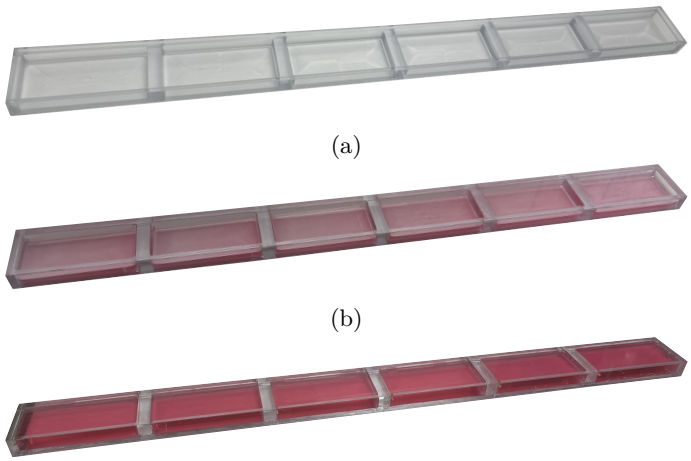

(a)

(b)

(c)

Fig. 1: Samples of hydroelastic PCs investigated in this work, with cavities: (a) lacking fluid, (b) partially filled, and (c) fully filled.

The remainder of this paper is organized as follows. Section 2 presents the mathematical modeling of hydroelastic PCs using reduced-order unit cell models and the WFEM. The results of numerical simulations are presented in Section 3. Finally, the main findings of this work are summarized in Section 4, followed by the acknowledgment and reference sections.

2 MODELING

This section presents the mathematical modeling of hydroelastic PCs using reduced-order unit cell models and the WFEM.

2.1 Full- and reduced-order finite element models of unit cells

Firstly, this subsection discusses the modeling of a single unit cell of a hydroelastic PC, including a MOR scheme.

Equations of motion The equations of motion for a single unit cell of a hydroelastic PC can be written as [5]:

$$\begin{bmatrix} \hat{\mathbf{M}}_{\mathrm{U}} & \mathbf{0} \\ \rho\,\hat{\mathbf{R}}^{\mathrm{T}} & \hat{\mathbf{M}}_{\mathrm{P}} \end{bmatrix} \begin{Bmatrix} \ddot{\hat{\mathbf{q}}}_{\mathrm{U}} \\ \ddot{\hat{\mathbf{q}}}_{\mathrm{P}} \end{Bmatrix} + \begin{bmatrix} \hat{\mathbf{K}}_{\mathrm{U}} & -\hat{\mathbf{R}} \\ \mathbf{0} & \hat{\mathbf{K}}_{\mathrm{P}} \end{bmatrix} \begin{Bmatrix} \hat{\mathbf{q}}_{\mathrm{U}} \\ \hat{\mathbf{q}}_{\mathrm{P}} \end{Bmatrix} = \begin{Bmatrix} \hat{\mathbf{f}}_{\mathrm{U}} \\ \hat{\mathbf{f}}_{\mathrm{P}} \end{Bmatrix}, \tag{1}$$

where $\hat{\mathbf{q}}_{\mathrm{U}}$ and $\hat{\mathbf{q}}_{\mathrm{P}}$ collect structural and pressure degrees of freedom (DoFs), respectively; $\hat{\mathbf{f}}_{\mathrm{U}}$ and $\hat{\mathbf{f}}_{\mathrm{P}}$ are load vectors applied to $\hat{\mathbf{q}}_{\mathrm{U}}$ and $\hat{\mathbf{q}}_{\mathrm{P}}$ DoFs, respectively; $\hat{\mathbf{M}}_j$ and $\hat{\mathbf{K}}_j$ ($j \in \{\mathrm{U}, \mathrm{P}\}$) stand for mass and stiffness matrices of structural (U) and acoustic (P) parts, respectively; $\hat{\mathbf{R}}$ stands for the fluid-structure coupling matrix; ρ is the fluid density; $(\ )^{\mathrm{T}}$ is the transpose operator; and $(\ddot{\ })$ represents second-order derivatives with respect to time. In partially filled cells, $\hat{\mathbf{M}}_{\mathrm{P}}$ in Eq. (1) is updated to account for linear fluid sloshing as follows: $\hat{\mathbf{M}}_{\mathrm{P}} \rightarrow \hat{\mathbf{M}}_{\mathrm{P}} + \hat{\mathbf{S}}_{\mathrm{P}}$, where $\hat{\mathbf{S}}_{\mathrm{P}}$ is the acoustic sloshing mass matrix [18].

The equations of motion of the unit cell are then partitioned according to the scheme illustrated in Fig. 2, where $\hat{\mathbf{q}}_{\mathrm{U}}$ and $\hat{\mathbf{q}}_{\mathrm{P}}$ are separated into sets of DoFs located at the left (L) and right (R) interfaces of the cell, as well as in its interior (I). These DoFs are further distinguished by their location at the fluid-structure interface, Γ, i.e., $\hat{\mathbf{q}}_{\Gamma_j}$ for $j \in \{\mathrm{L}, \mathrm{R}, \mathrm{I}\}$. Each set of DoFs at the fluid-structure interface is further divided into structural and acoustic parts, i.e., $\hat{\mathbf{q}}_{\Gamma_{\mathrm{L}}} = \{\hat{\mathbf{q}}^{\mathrm{T}}_{\Gamma_{\mathrm{L,U}}}\ \hat{\mathbf{q}}^{\mathrm{T}}_{\Gamma_{\mathrm{L,P}}}\}^{\mathrm{T}}$, $\hat{\mathbf{q}}_{\Gamma_{\mathrm{R}}} = \{\hat{\mathbf{q}}^{\mathrm{T}}_{\Gamma_{\mathrm{R,U}}}\ \hat{\mathbf{q}}^{\mathrm{T}}_{\Gamma_{\mathrm{R,P}}}\}^{\mathrm{T}}$, and $\hat{\mathbf{q}}_{\Gamma_{\mathrm{I}}} = \{\hat{\mathbf{q}}^{\mathrm{T}}_{\Gamma_{\mathrm{I,U}}}\ \hat{\mathbf{q}}^{\mathrm{T}}_{\Gamma_{\mathrm{I,P}}}\}^{\mathrm{T}}$.

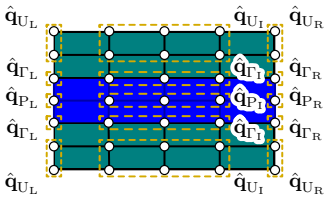

Fig. 2: Partitioning of DoFs based on node location (L, R, and I) and medium type (U and P) for the finite element mesh of a unit cell of a hydroelastic PC.

In accordance with the previous partitioning, Eq. (1) is rewritten as follows:

$$\hat{\mathbf{M}}\ddot{\hat{\mathbf{q}}} + \hat{\mathbf{K}}\hat{\mathbf{q}} = \hat{\mathbf{f}}, \tag{2}$$

where:

$$\hat{\mathbf{q}} = \left\{\hat{\mathbf{q}}^{\mathrm{T}}_{\mathrm{U_L}}\ \hat{\mathbf{q}}^{\mathrm{T}}_{\mathrm{P_L}}\ \hat{\mathbf{q}}^{\mathrm{T}}_{\Gamma_{\mathrm{L}}}\ \hat{\mathbf{q}}^{\mathrm{T}}_{\mathrm{U_R}}\ \hat{\mathbf{q}}^{\mathrm{T}}_{\mathrm{P_R}}\ \hat{\mathbf{q}}^{\mathrm{T}}_{\Gamma_{\mathrm{R}}}\ \hat{\mathbf{q}}^{\mathrm{T}}_{\mathrm{U_I}}\ \hat{\mathbf{q}}^{\mathrm{T}}_{\mathrm{P_I}}\ \hat{\mathbf{q}}^{\mathrm{T}}_{\Gamma_{\mathrm{I}}}\right\}^{\mathrm{T}}, \tag{3}$$

$$\hat{\mathbf{f}} = \left\{\hat{\mathbf{f}}^{\mathrm{T}}_{\mathrm{U_L}}\ \hat{\mathbf{f}}^{\mathrm{T}}_{\mathrm{P_L}}\ \hat{\mathbf{f}}^{\mathrm{T}}_{\Gamma_{\mathrm{L}}}\ \hat{\mathbf{f}}^{\mathrm{T}}_{\mathrm{U_R}}\ \hat{\mathbf{f}}^{\mathrm{T}}_{\mathrm{P_R}}\ \hat{\mathbf{f}}^{\mathrm{T}}_{\Gamma_{\mathrm{R}}}\ \hat{\mathbf{f}}^{\mathrm{T}}_{\mathrm{U_I}}\ \hat{\mathbf{f}}^{\mathrm{T}}_{\mathrm{P_I}}\ \hat{\mathbf{f}}^{\mathrm{T}}_{\Gamma_{\mathrm{I}}}\right\}^{\mathrm{T}}. \tag{4}$$

Reduction of $\hat{\mathbf{q}}_{\mathbf{U_I}}$ and $\hat{\mathbf{q}}_{\mathbf{P_I}}$ DoFs using the CB method The set of DoFs $\hat{\mathbf{q}}_{\mathrm{U_I}}$ and $\hat{\mathbf{q}}_{\mathrm{P_I}}$ in Fig. 2 are uncoupled from each other due to the fluid structure interface between them. Therefore, their reduction can be performed using an adapted version of the Craig-Bampton (CB) MOR method [19]:

$$\hat{\mathbf{q}} = \boldsymbol{\alpha}_{\mathrm{CB}} \tilde{\mathbf{q}}, \tag{5}$$

where:

$$\tilde{\mathbf{q}} = \left\{ \hat{\mathbf{q}}_{\mathrm{U_L}}^{\mathrm{T}} \; \hat{\mathbf{q}}_{\mathrm{P_L}}^{\mathrm{T}} \; \hat{\mathbf{q}}_{\Gamma_{\mathrm{L}}}^{\mathrm{T}} \; \hat{\mathbf{q}}_{\mathrm{U_R}}^{\mathrm{T}} \; \hat{\mathbf{q}}_{\mathrm{P_R}}^{\mathrm{T}} \; \hat{\mathbf{q}}_{\Gamma_{\mathrm{R}}}^{\mathrm{T}} \; \mathbf{q}_{\mathrm{U_I}}^{\mathrm{T}} \; \mathbf{q}_{\mathrm{P_I}}^{\mathrm{T}} \; \hat{\mathbf{q}}_{\Gamma_{\mathrm{I}}}^{\mathrm{T}} \right\}^{\mathrm{T}}, \tag{6}$$

$\mathbf{q}_{\mathrm{U_I}}$ and $\mathbf{q}_{\mathrm{P_I}}$ denote vectors in modal coordinates related to their physical counterparts $\hat{\mathbf{q}}_{\mathrm{U_I}}$ and $\hat{\mathbf{q}}_{\mathrm{P_I}}$, and $\boldsymbol{\alpha}_{\mathrm{CB}}$ represents the CB projection matrix (including fixed-interface modes and static/constraint modes).

Using Eq. (5) and pre-multiplying Eq. (2) by $\boldsymbol{\alpha}_{\mathrm{CB}}^{\mathrm{T}}$, one obtains:

$$\tilde{\mathbf{M}} \ddot{\tilde{\mathbf{q}}} + \tilde{\mathbf{K}} \tilde{\mathbf{q}} = \tilde{\mathbf{f}}, \tag{7}$$

where $\tilde{\mathbf{M}} = \boldsymbol{\alpha}_{\mathrm{CB}}^{\mathrm{T}} \hat{\mathbf{M}} \boldsymbol{\alpha}_{\mathrm{CB}}$, $\tilde{\mathbf{K}} = \boldsymbol{\alpha}_{\mathrm{CB}}^{\mathrm{T}} \hat{\mathbf{K}} \boldsymbol{\alpha}_{\mathrm{CB}}$, and $\tilde{\mathbf{f}} = \boldsymbol{\alpha}_{\mathrm{CB}}^{\mathrm{T}} \hat{\mathbf{f}}$.

Reduction of $\hat{\mathbf{q}}_{\mathbf{\Gamma_I}}$ DoFs using an local-level characteristic constraint (L-CC) MOR method The reduction of DoFs collected in $\hat{\mathbf{q}}_{\Gamma_{\mathrm{I}}}$ can be performed using the L-CC MOR method [20]:

$$\tilde{\mathbf{q}} = \boldsymbol{\alpha}_{\text{L-CC}_{\Gamma_{\mathrm{I}}}} \bar{\mathbf{q}}, \tag{8}$$

where:

$$\bar{\mathbf{q}} = \left\{ \hat{\mathbf{q}}_{\mathrm{U_L}}^{\mathrm{T}} \; \hat{\mathbf{q}}_{\mathrm{P_L}}^{\mathrm{T}} \; \hat{\mathbf{q}}_{\Gamma_{\mathrm{L}}}^{\mathrm{T}} \; \hat{\mathbf{q}}_{\mathrm{U_R}}^{\mathrm{T}} \; \hat{\mathbf{q}}_{\mathrm{P_R}}^{\mathrm{T}} \; \hat{\mathbf{q}}_{\Gamma_{\mathrm{R}}}^{\mathrm{T}} \; \mathbf{q}_{\mathrm{U_I}}^{\mathrm{T}} \; \mathbf{q}_{\mathrm{P_I}}^{\mathrm{T}} \; \mathbf{q}_{\Gamma_{\mathrm{I}}}^{\mathrm{T}} \right\}^{\mathrm{T}}, \tag{9}$$

$\mathbf{q}_{\Gamma_{\mathrm{I}}}$ denotes a vector in modal coordinates related to its physical counterpart $\hat{\mathbf{q}}_{\Gamma_{\mathrm{I}}}$, and $\boldsymbol{\alpha}_{\text{L-CC}_{\Gamma_{\mathrm{I}}}}$ is the L-CC projection matrix, derived similarly to [21].

Thus, using Eq. (8) and pre-multiplying Eq. (7) by $\boldsymbol{\alpha}_{\text{L-CC}_{\Gamma_{\mathrm{I}}}}^{\mathrm{T}}$, one derives:

$$\bar{\mathbf{M}} \ddot{\bar{\mathbf{q}}} + \bar{\mathbf{K}} \bar{\mathbf{q}} = \bar{\mathbf{f}}, \tag{10}$$

where $\bar{\mathbf{M}} = \boldsymbol{\alpha}_{\text{L-CC}_{\Gamma_{\mathrm{I}}}}^{\mathrm{T}} \tilde{\mathbf{M}} \boldsymbol{\alpha}_{\text{L-CC}_{\Gamma_{\mathrm{I}}}}$, $\bar{\mathbf{K}} = \boldsymbol{\alpha}_{\text{L-CC}_{\Gamma_{\mathrm{I}}}}^{\mathrm{T}} \tilde{\mathbf{K}} \boldsymbol{\alpha}_{\text{L-CC}_{\Gamma_{\mathrm{I}}}}$, and $\bar{\mathbf{f}} = \boldsymbol{\alpha}_{\text{L-CC}_{\Gamma_{\mathrm{I}}}}^{\mathrm{T}} \tilde{\mathbf{f}}$.

Reduction of boundary DoFs using an L-CC MOR method The reduction of boundary DoFs is also performed using the L-CC MOR method [22]:

$$\bar{\mathbf{q}} = \boldsymbol{\alpha}_{\text{L-CC}_{\mathrm{B}}} \mathbf{q}, \tag{11}$$

where:

$$\mathbf{q} = \left\{ \mathbf{q}_{\mathrm{U_L}}^{\mathrm{T}} \; \mathbf{q}_{\mathrm{P_L}}^{\mathrm{T}} \; \mathbf{q}_{\Gamma_{\mathrm{L}}}^{\mathrm{T}} \; \mathbf{q}_{\mathrm{U_R}}^{\mathrm{T}} \; \mathbf{q}_{\mathrm{P_R}}^{\mathrm{T}} \; \mathbf{q}_{\Gamma_{\mathrm{R}}}^{\mathrm{T}} \; \mathbf{q}_{\mathrm{U_I}}^{\mathrm{T}} \; \mathbf{q}_{\mathrm{P_I}}^{\mathrm{T}} \; \mathbf{q}_{\Gamma_{\mathrm{I}}}^{\mathrm{T}} \right\}^{\mathrm{T}}, \tag{12}$$

$\mathbf{q}_{\mathrm{U_L}}$, $\mathbf{q}_{\mathrm{P_L}}$, $\mathbf{q}_{\Gamma_{\mathrm{L}}}$, $\mathbf{q}_{\mathrm{U_R}}$, $\mathbf{q}_{\mathrm{P_R}}$, and $\mathbf{q}_{\Gamma_{\mathrm{R}}}$ denote vectors in modal coordinates corresponding to their physical counterparts $\hat{\mathbf{q}}_{\mathrm{U_L}}$, $\hat{\mathbf{q}}_{\mathrm{P_L}}$, $\hat{\mathbf{q}}_{\Gamma_{\mathrm{L}}}$, $\hat{\mathbf{q}}_{\mathrm{U_R}}$, $\hat{\mathbf{q}}_{\mathrm{P_R}}$, and $\hat{\mathbf{q}}_{\Gamma_{\mathrm{R}}}$, respectively, and $\boldsymbol{\alpha}_{\text{L-CC}_{\mathrm{B}}}$ is the L-CC projection matrix.

Hence, using Eq. (11), and pre-multiplying Eq. (10) by $\boldsymbol{\alpha}_{\text{L-CC}_{\mathrm{B}}}^{\mathrm{T}}$, yields:

$$\mathbf{M} \ddot{\mathbf{q}} + \mathbf{K} \mathbf{q} = \mathbf{f}, \tag{13}$$

where $\mathbf{M} = \boldsymbol{\alpha}_{\text{L-CC}_{\mathrm{B}}}^{\mathrm{T}} \bar{\mathbf{M}} \boldsymbol{\alpha}_{\text{L-CC}_{\mathrm{B}}}$, $\mathbf{K} = \boldsymbol{\alpha}_{\text{L-CC}_{\mathrm{B}}}^{\mathrm{T}} \bar{\mathbf{K}} \boldsymbol{\alpha}_{\text{L-CC}_{\mathrm{B}}}$, and $\mathbf{f} = \boldsymbol{\alpha}_{\text{L-CC}_{\mathrm{B}}}^{\mathrm{T}} \bar{\mathbf{f}}$.

2.2 The WFEM applied to hydroelastic PCs

The application of the WFEM [23,24] to reduced-order unit cell models of hydroelastic PCs can be performed as summarized next.

First, Eq. (13) is reformulated by considering $\mathbf{q}_{\mathrm{P}} = -\rho\dot{\mathbf{q}}_{\varphi}$, where $\mathbf{q}_{\varphi}$ denotes the acoustic velocity potential [25]. Afterwards, it is recast in the frequency domain, yielding the following eigenvalue problem after further manipulations:

$$\left(\mathbf{S} - \mu_j \mathbf{I}\right) \boldsymbol{\phi}_j = \mathbf{0}, \tag{14}$$

where $\mathbf{S}$ is the unit cell transfer matrix, and μ_j and $\boldsymbol{\phi}_j$ are wave modes (propagation constants and wave shapes, respectively). Bloch wavenumbers are obtained as $k_j = (\ln \mu_j)/(-\mathrm{i}\Delta)$, where Δ is the unit cell length in the direction of wave propagation. To address numerical issues in solving Eq. (14), various approaches exist in the literature — the $\mathbf{S} + \mathbf{S}^{-1}$ have been used in this work [23].

Wave modes from Eq. (14) can then be used to calculate forced responses of finite hydroelastic periodic structures upon enforcing boundary conditions [24]. Thereafter, responses in physical coordinates can be retrieved.

3 RESULTS

The following subsections present the results of numerical simulations conducted to: (1) verify the reduced-order unit cell models derived in accordance with Subsection 2.1; and (2) investigate the dynamic behavior of hydroelastic PCs under varying fluid filling levels.

Simulations were performed considering a hydroelastic PC with unit cells measuring 60 mm × 10 mm × 30 mm (Δ = 60 mm), each featuring a perfectly centered internal void with dimensions 53.6 mm × 6 mm × 23.6 mm [17]. Several fluid filling levels are considered, namely 0 mm (empty), 1 mm, 2 mm, 3 mm, 4 mm, 5 mm, and 6 mm (completely filled) — Fig. 1 illustrates three of these conditions. The structural material is polycarbonate, with an elastic modulus of 2.64 GPa, a density of 1200kg m^{-3}, and a Poisson's ratio of 0.38, while the fluid is water, with a density of 998.2 kg m^{-3} and a sound velocity of 1482.1 m s^{-1}. Dissipation effects are accounted for only in the polycarbonate, where $\mathbf{K}_{\mathrm{U}} \rightarrow (1 + i\eta)\mathbf{K}_{\mathrm{U}}$ in Eq. (13), with η = 1%. For all scenarios, finite elements with quadratic interpolation functions and an element size of 2.5 mm are employed. The maximum frequency of interest is limited to 5000 Hz.

3.1 Model verification

First of all, Fig. 3 shows frequency response functions (FRFs) computed using the WFEM with reduced-order unit cell models, and the FEM, for finite hydroelastic PCs with six unit cells, considering fluid fillings of 1 mm, 3 mm and 5 mm — results for other fluid fillings are omitted for brevity. As one may notice, the FRFs obtained from the WFEM closely match those computed using full FEM models. In all cases, reductions from physical to modal equations of more than 93% were achieved, along with decreases in computation time exceeding 100-fold, demonstrating the great performance of the proposed MOR approach.

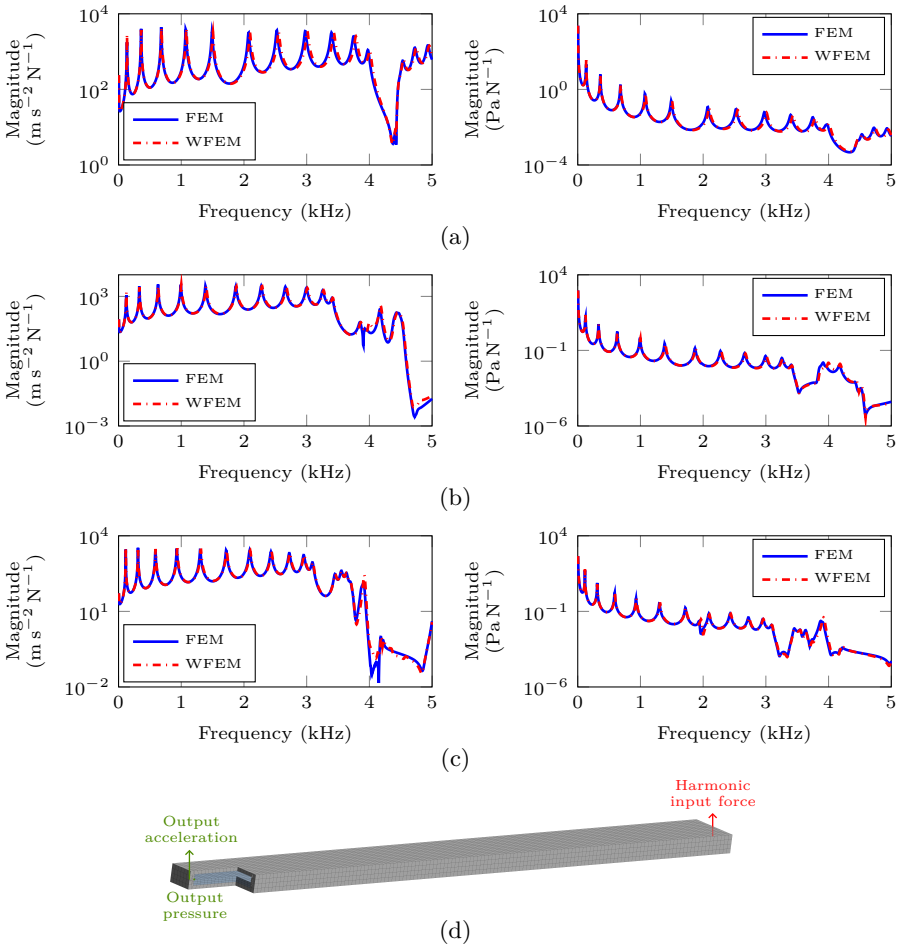

Fig. 3: Frequency response functions computed using the WFEM, with reduced-order unit cell models, and the FEM for three different fluid filling conditions: (a) 1 mm, (b) 3 mm, and (c) 5 mm. In all cases, the output acceleration occurs at the DoF indicated in (d), while the fluid response is calculated at the fluid free surface, as schematized in the same subfigure for the case with 3 mm filling.

3.2 On the wave propagation in hydroelastic PCs

We now investigate wave propagation through the hydroelastic PCs. First, Fig. 4 presents dispersion curves and FRFs obtained for an empty and a fully filled PC. For the calculation of FRFs, the same input and output (acceleration) locations shown in Fig. 3d are considered. As one may notice in Fig. 4, the bending bandgaps predicted by the Bloch-Floquet theorem for infinite PCs align with the stopbands observed in the FRFs. In addition, Fig. 4 shows that fluid inclusion increases inertia, thereby shifting all bandgaps to lower frequencies.

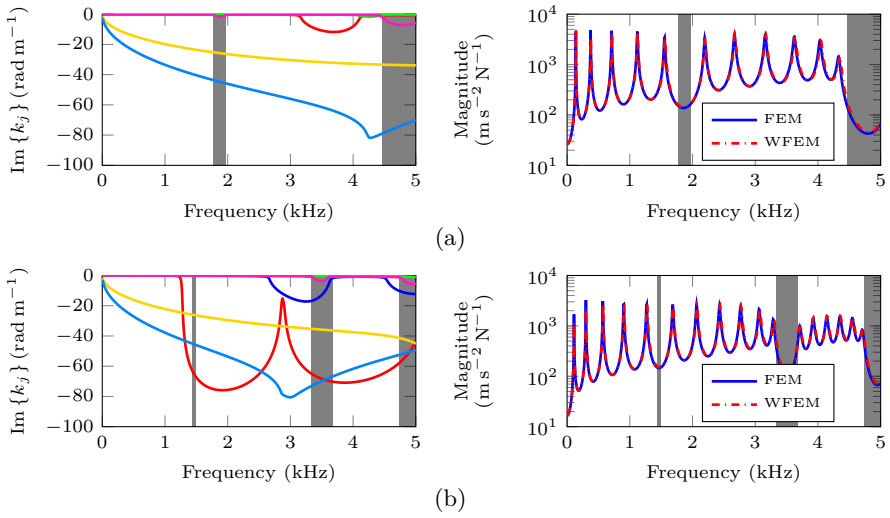

Fig. 4: Dispersion curves (left) and FRFs (right) calculated for (a) empty and (b) fully filled PCs (6 mm). For the calculation of FRFs, the same input and output (acceleration) locations shown in Fig. 3d are considered.

To assess the impact of fluid filling on the dynamic behavior of hydroelastic PCs, Fig. 5 presents FRFs for various fillings, based on the input and output (acceleration) locations shown in Fig. 3d, with colors indicating the amplitude of vibration. First, Fig. 5 shows that partially filled hydroelastic PCs exhibit distinct changes in their responses compared to the empty and fully filled cases. They appear to display more frequency bands where wave propagation is forbidden due to bandgap formation, especially for higher fluid fillings. It is also evident from Fig. 5 that wave propagation can be manipulated by adjusting the fluid level, opening new avenues for the design of tunable periodic structures.

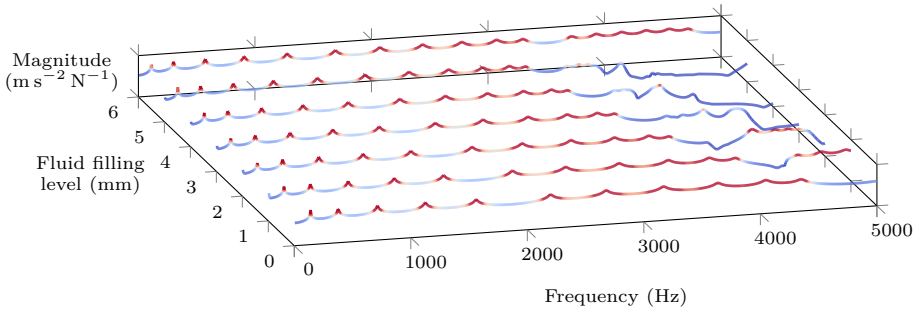

Fig. 5: Magnitude of accelerance FRFs computed using WFEM with reduced-order unit cell models, for locations indicated in Fig. 3d and various fluid levels.

4 CONCLUDING REMARKS

This paper presented a modeling framework for hydroelastic PCs, combining reduced-order unit cell models with the WFEM, and investigated the influence of fluid filling levels on their dynamic behavior. Numerical simulations demonstrated that the forced responses obtained using the reduced-order unit cell models and the WFEM are in very good agreement with reference results from traditional FEM. The proposed framework led to substantial reductions in computational time and model size, further highlighting its capability for the efficient and accurate analysis of hydroelastic periodic structures. Dispersion analyses and FRFs showed that fluid inclusion significantly modifies wave propagation in hydroelastic PCs, shifting stopbands and enhancing bandgap formation. These findings open new avenues for the design of advanced metastructures with strong potential for wave manipulation, including tunable bandgaps and waveguides, adaptive vibration control, reconfigurability, and other functions.

5 ACKNOWLEDGEMENTS

This study was financed, in part, by the São Paulo Research Foundation (FAPESP), Brasil. Process Numbers #2018/15894-0, #2023/11207-7 and #2024/07549-2. All authors are grateful to FAPESP for the provided grants. V. M. S. Santos also acknowledges the Brazilian Coordination for the Improvement of Higher Education Personnel (CAPES). M. Ouisse acknowledges the graduate school EIPHI (project ANR-17-EURE-0002).

References

1. Khelif, A., Choujaa, A., Benchabane, S., Djafari-Rouhani, B., Laude, V.: Guiding and bending of acoustic waves in highly confined phononic crystal waveguides. Appl. Phys. Lett. **84**(22), 4400–4402 (2004)
2. Li, J.B., Wang, Y.S., Zhang, C.: Dispersion relations of a periodic array of fluid-filled holes embedded in an elastic solid. J. Comput. Acoust. **20**(04), 1250014 (2012)
3. Spadoni, A., Höhler, R., Cohen-Addad, S., Dorodnitsyn, V.: Closed-cell crystalline foams: Self-assembling, resonant metamaterials. J. Acoust. Soc. Am. **135**(4), 1692–1699 (2014)
4. Dorodnitsyn, V., Spadoni, A.: Elasto-Dynamic Behavior of a Two-Dimensional Square Lattice With Entrained Fluid II: Microstructural and Homogenized Models. J. Vib. Acoust. **136**(3) (2014)
5. Dorodnitsyn, V., Spadoni, A.: Elastodynamics of a Two-Dimensional Square Lattice With Entrained Fluid — Part I: Comparison With Biot's Theory. J. Vib. Acoust. **136**(2) (2014)
6. Dorodnitsyn, V., Damme, B.V.: Two-dimensional fluid-filled closed-cell cellular solid as an acoustic metamaterial with negative index. Phys. Rev. B **93**(13), 134302 (2016)
7. Jensen, J.S., Kook, J.: Coupled Acoustic-Mechanical Bandgaps. Crystals **6**(9), 112 (2016)

8. Wang, T.T., Wang, Y.F., Wang, Y.S., Laude, V.: Tunable fluid-filled phononic metastrip. Appl. Phys. Lett. **111**(4), 041906 (2017)
9. Wang, Y.F., Wang, T.T., Wang, Y.S., Laude, V.: Reconfigurable Phononic-Crystal Circuits Formed by Coupled Acoustoelastic Resonators. Phys. Rev. Appl. **8**(1), 014006 (2017)
10. Zhang, Q., Zhang, K., Hu, G.: Tunable fluid-solid metamaterials for manipulation of elastic wave propagation in broad frequency range. Appl. Phys. Lett. **112**(22), 221906 (2018)
11. Elmadih, W., Chronopoulos, D., Zhu, J.: Metamaterials for simultaneous acoustic and elastic bandgaps. Sci. Rep. **11**, 14635 (2021)
12. Yu, D., Wen, J., Zhao, H., Liu, Y., Wen, X.: Vibration reduction by using the idea of phononic crystals in a pipe-conveying fluid. J. Sound Vib. **318**(1-2), 193–205 (2008)
13. Dai, H.L., Wang, L., Ni, Q.: Dynamics of a fluid-conveying pipe composed of two different materials. Int. J. Eng. Sci. **73**, 67–76 (2013)
14. Yu, D.L., Shen, H.J., Liu, J.W., Yin, J.F., Zhang, Z.F., Wen, J.H.: Propagation of acoustic waves in a fluid-filled pipe with periodic elastic Helmholtz resonators. Chin. Phys. B **27**(6), 064301 (2018)
15. Hu, B., Zhang, Z., Yu, D., Liu, J., Zhu, F.: Broadband bandgap and shock vibration properties of acoustic metamaterial fluid-filled pipes. J. Appl. Phys. **128**(20), 205103 (2020)
16. Song, Y., Shen, Y.: Highly morphing and reconfigurable fluid-solid interactive metamaterials for tunable ultrasonic guided wave control. Appl. Phys. Lett. **121**(26), 264102 (2022)
17. Santos, V.M.S., Sales, T.P., Ouisse, M.: Investigation of a novel metastructure with trapped, fluid-filled unit cells. In: Kurka, P., Pereira, M. (eds.) Advances in Structural Vibration. Lecture Notes in Mechanical Engineering. Springer (2024)
18. Ansys®: Mechanical APDL 2024 R2, Release 24.2, Theory Reference, Acoustic Fluid-Structure Interaction (FSI), ANSYS, Inc. (2024)
19. Craig, R.R., Bampton, M.C.C.: Coupling of substructures for dynamic analyses. AIAA J. **6**(7), 1313–1319 (1968)
20. Krattiger, D., Hussein, M.I.: Generalized Bloch mode synthesis for accelerated calculation of elastic band structures. J. Comput. Phys. **357**, 183–205 (2018)
21. Maess, M., Gaul, L.: Substructuring and model reduction of pipe components interacting with acoustic fluids. Mech. Syst. Signal Pr. **20**(1), 45–64 (2006)
22. Santos, V.M.S., Sales, T.P., Ouisse, M.: Improving the computation of forced responses of periodic structures by the wave-based finite element method via a modified generalized Bloch mode synthesis. Finite Elem. Anal. Des. **245**, 104314 (2025)
23. Mencik, J.M., Duhamel, D.: A wave-based model reduction technique for the description of the dynamic behavior of periodic structures involving arbitrary-shaped substructures and large-sized finite element models. Finite Elem. Anal. Des. **101**, 1–14 (2015)
24. Hoang, T., Duhamel, D., Foret, G.: Wave finite element method for waveguides and periodic structures subjected to arbitrary loads. Finite Elem. Anal. Des. **179**, 103437 (2020)
25. Everstine, G.C.: A symmetric potential formulation for fluid-structure interaction. J. Sound Vib. **79**(1), 157–160 (1981)